Structural, Optical and Microwave Dielectric Properties of $Ba(Ti_{1-x}Sn_x)_4O_9$, $0 \leq x \leq 0.7$ Ceramics

Asad Ali
Riphah International University
Sarir Uddin
Government Degree College Hayatabad
Madan Lal (madan.physics6@gmail.com)
Eternal University
Abid Zaman
Riphah International University
Zafar Iqbal
Riphah International University
Khaled Althubeiti
Taif University

Research Article

Keywords: X-ray diffraction (XRD), Grain size, Scanning electron microscopy (SEM, Optical properties,), Dielectric properties.

Posted Date: June 7th, 2021

DOI: https://doi.org/10.21203/rs.3.rs-566760/v1

Abstract

Sn-doped $BaTi_4O_9$ (BT4) microwave ceramics were prepared by a mixed oxide route. Preliminary X-ray diffraction (XRD) structural study shows that the samples have orthorhombic symmetry with space group (Pnmm). Scanning electron microscopy (SEM) shows that the grain size of the samples decreases with increasing Sn^{4+} contents. The presence of the metal oxide efficient group was revealed by Fourier transform infrared (FTIR) spectroscopy. The Photoluminescence spectra of the samples reported red color ~ 603, 604, 606.5 and 605 nm with excitation energy ~ 2.06, 2.05, 2.04 and 2.05 eV for Sn content at x = 0.0, 0.3, 0.5, and 0.7, respectively. The microwave dielectric properties of all the samples were investigated by an impedance analyzer. The excellent microwave dielectric properties i.e. high relative permittivity (ε_r = 57.29), high-quality factor (Q_f = 11,852), and low-dielectric loss (3.007) has been observed.

Introduction

Dielectric materials are frequently used in modern telecommunication systems like satellite modules and cellular phones. Dielectric layered-structured materials have been widely investigated for their potential use in ferroelectric random access memories (FeRAM) and piezoelectric devices. Ferroelectric and piezoelectric ceramics are broadly used in a range of applications such as sensors, actuators, transducers, pulse signal circuits, spacecraft, X-ray equipment, weapons, medical devices, and transportation. The dielectric component used in these devices is termed dielectric resonators (DR). The optimum commercial properties of these ceramics included the excellent dielectric constant (ε_r), good quality factor (Q_f) or low tangent loss (tan σ), and near to zero temperature coefficient at resonant frequency (τ_f)[1-6]. For example, a dielectrically loaded antenna requires; ε_r from 20 to 85, (Q) ≥ 10,000, and τ_f close to zero[7,8]. Some time quality factors can be expressed in the product of Q and f_o (resonant frequency) i.e. ($Q \times f_o$). The dielectric constant and dielectric loss (tan σ) decreases with a resonant frequency, which suggests that electric dipoles and interfaces play a key role at lower frequencies. The decrease in dielectric constant with resonant frequency can be explained based on Koops theory reported by K. Praveena and K. B. R. Varma[9]. A relatively good dielectric constant is required for the miniaturization of devices and low tangent loss is required for noise reduction while zero τ_f is important for temperature stability of the DR[2]. From the manufacturing point of view, it is very difficult to obtain compounds with all three optimum properties along with a low cost. Among oxides compounds, $BaTi_4O_9$ (BT4) is one of the dielectric materials that may be used in the microwave domain reported first by Rase and Roy[10]. It has been recorded that BaTi4O9 ceramics have ε_r = 37.3, Q = 27200 GHz and τ_f = +15 ppm/°C[11]. On the other side, wet chemical methods (i.e. sol-gel, co-precipitation, or hydrothermal) can be used for the preparation of titanates ceramics[12]. The optical, structural, microstructural, and microwave properties of $BaTi_4O_9$ ceramic samples with various dopant elements have been studied at microwave frequency. Many researchers studied the effects of B site cation substitutions. Dielectric properties of the sample may be affected by the substitution of larger ionic radius (Sn^{4+}) for smaller ionic radius (Ti^{4+})

ions[13-15]. In this way Veenhuis et al processed compounds with good dielectric properties which have been used in the field of advanced laser technology and optical storage devices[16].

In the present decade, BT4 has been investigated broadly because of its good Q_f, high ε_r, and small τ_f. Hence, widely used in microwave dielectric resonator applications, patch antenna, microwave telecommunication, etc. During the densification of these titanates at very high sintering temperatures, enhanced dielectric properties are observed due to the structural and compositional defects (fluctuations) because of the substitution of Ti^{4+} ion for Ti^{3+} ion[17]. The present work aims to achieve a material with enhanced structural and electrical properties for device application. In this report, we describe the preparation of $Ba(Ti_{1-x}Sn_x)_4O_9$ ceramics by the mixed oxide method. The calcined powders and sintered products obtained were characterized by XRD (X-ray diffraction), SEM (scanning electron microscopy), impedance analyzer, and FTIR (Fourier transform infra-red). The microwave dielectric properties of samples are discussed in terms of their physical and chemical characteristics.

Materials And Methods

The starting raw materials were: $BaCO_3$ (Merck, Germany, 99.9%), TiO_2 (Aldrich Chemical Company, Inc., U.S.A, 99.9%), and SnO_2 (Strem, Chemicals, U.S.A, 99.9%) to make solid solutions of $Ba(Ti_{1-x}Sn_x)_4O_9$, $0 \leq x \leq 0.7$ by the conventional mixed oxides route. These raw materials were balanced according to stoichiometric ratio and mixed for 12 hours in distilled water by using horizontal ball milling. Then the slurry was dried in a microwave oven at 100 °C for one day and calcined at 1100 °C for 3 h in a nickel crucible in the air atmosphere with a heating-cooling rate of 10 °C/min. The calcined powders were grinded for 60 mins with a mortar and pistol manually to avoid agglomerations. Then pressed 0.6-0.8 gm of powder into cylindrical pellets of thickness 2 mm and diameter 10 mm by using a hydraulic press (CARVER, USA) with a pressure of 80 MPa. Thereafter the pellets were sintered at 1320 °C temperature in the open air for 2 h with a heating-cooling rate of 10 °C/min. The XRD patterns of the compounds were recorded at room temperature using an X-ray powder diffractometer (JDX-3532, JEOL, Japan) with Cu Ka radiation (k = 1.5405 Å) in a wide range of Bragg angles 2h ($20^\circ \leq 2\theta \leq 60^\circ$) at a scanning rate of 2 deg min^{-1}. The experimental density of the samples was measured by the archimedus principle using a density meter (MD-3005, Germany). Scanning electron microscopy (SEM, JEOL 7600F) can be used to study the microstructure of the dense pellets. To obtain 10 cm^{-1} resolution spectra of the pellets were carried out by using the Fourier transformation infrared spectroscopy (FTIR, Perkin-Elmer).

Results And Discussions

XRD analysis

Figure 1 represents the room temperature XRD patterns of $Ba(Ti_{1-x}Sn_x)_4O_9$, $0 \leq x \leq 0.7$ ceramics. The mean peaks corresponding to (200), (121), (150), (211), (230), (320), (213), and (503) planes are well-matched with PDF card number 34-70 of $BaTi_4O_9$ ceramics and have an orthorhombic structure with

space group (Pnmm). Some of the secondary phases of $Ba_2Ti_8O_{18}$ are detectable and matched with PDF card number 0080-0916. It can be noted from Figure 1 that the peaks shifted toward the lower 2θ values representing expansion in the lattice cell volume as the Sn^{4+} contents increase in ceramics. This might be due to the inhomogeneity, microstrain, or maybe due to the substitution of the relatively larger cation ion of Sn^{4+} (~0.69 Å) for a lower cation ion of Ti^{4+} (~0.64 Å)[18]. The calculated lattice parameters (i.e. 'a', 'b', and 'c') from the X-ray diffraction show increase in their values as Sn^{4+} content increased. This increase in the lattice parameters, resulting in the phase transition from orthorhombic to a tetragonal structure. The average crystallite size of each ceramics was calculated by using Debye Scherer's formula[19] and the observed average crystallite size and various lattice parameters are listed in Table 1.

$$\text{Crystallite size, } D = \frac{0.9\lambda}{\beta \text{Cos}\theta} \qquad (1)$$

Microstructure analysis

SEM images were used to calculate the average grain size and density of $Ba(Ti_{1-x}Sn_x)_4O_9$, $0 \leq x \leq 0.7$ ceramics (as shown in Figure 2). It can be noted that two types of morphologies present in all samples-rodlike and spherical shape particles. The relative population is increased when the Sn^{4+} doping content is increased in the base sample. The existence of cavities in the denser pellets confirms the existence of porosity. Thus, an increase in the relative density and decrease in the porosity was observed as the Sn content increased[20]. The porosity of the samples was calculated using equation (2) shown in Table 2.

$$\text{Porosity} = \left(\frac{\rho_{th} - \rho_{ex}}{\rho_{th}}\right) \times 100\% \qquad (2)$$

Where ρ_{th} = theoretical density and ρ_{ex} = experimental density (calculated using Archimede's principle). The observed average grain size varies in the decreasing order ~10.7 to ~2 μm as dopant content x varies from 0.0 to 0.7. At x = 0.5 Sn^{4+} doped $BaTi_4O_9$ system have smaller average grain size, gives rise to a more uniform grain size distribution with an overall average grain size of 0.8 μm. Thus, high densification (~99.4%) and low porosity (~0.55 %) were achieved with Sn^{4+} content which tends to reduce grain growth.

Optical properties

The FTIR spectra of $Ba(Ti_{1-x}Sn_x)_4O_9$, $0 \leq x \leq 0.7$ ceramics at room temperature as shown in Figure 3. The peaks that appear near ~2852, ~2922, and ~1433 cm^{-1} represents the symmetric, asymmetric, and bending vibrations of the $-CH_2$ group, respectively[21]. Peaks appearing at ~854 cm^{-1} show the vibrational mode which relates to the stretching mode of the O-Ti-O system in the samples that confirms the presence of the $BaTi_4O_9$ structures[22]. The absorption mode appearing at ~690 cm^{-1} shows the Ti-O stretching mode of the octahedral group in complex perovskite structure[23,24], as this mode appears only

in $BaTi_4O_9$ ceramic samples. Furthermore, the structure of the $BaTi_4O_9$ ceramic sample has been confirmed by the XRD result.

Photoluminescence spectroscopy of $Ba(Ti_{1-x}Sn_x)_4O_9$, $0 \leq x \leq 0.7$ calcined ceramics is shown in Figure 4. This optical emission spectra are recognized as the recombination of electrons and holes in the state of transfer of carrier ions. By using equation (3), we can find the value of excitation energy of the samples.

$$E = hc/\lambda \qquad (3)$$

Where, E = optical excitation energy, h = Plank's constant (~6.63 x 10^{-34} Js) c = velocity of light (3 x 10^8 m/s) and λ is the emission wavelength. Emission at photoluminescence peak of the samples were recorded at ~603, 604, 606.5 and 605 nm with excitation energy ~2.06, 2.05, 2.04 and 2.05 eV for x = 0.0, 0.3, 0.5, and 0.7 content of Sn, respectively. Photoluminescence is a multiphotonic process that is an optical energy emission occurred in the optical gape by many vibrational modes within the sample[25]. Within the energy bandgap, the photoluminescence process confirmed that due to localizing state the order/disorder structure may be affected directly. Hence, the structural order may be increased with increasing the energy band gap[26]. It has been recorded that a broad-emission spectrum was located at ~604 nm and have an optical excitation energy (~2.06 eV) which is smaller than the energy band gap of extremely ordered $BaTi_4O_9$ located at ~558 nm (~2.23 eV) which is maybe the absence of the oxygen vacancy[27]. In the photoluminescence spectrum, the red color may occur due to the oxygen vacancy.

Microwave dielectric properties

The variation of the relative permittivity (ε_r) and tangent loss (tanδ) of $Ba(Ti_{1-x}Sn_x)_4O_9$, $0 \leq x \leq 0.7$ ceramics versus frequency at room temperature is shown in Figure 5. Due to increasing frequency, the values of ε_r and tanδ decrease exponentially in the samples. The high value of ε_r at a resonant frequency can be described based on (i) according to Maxwell-Wagner's model the dielectric materials are consist of fine conductive grains which are surrounded by grain boundaries. Large polarization is caused by the motion of charge carriers from grain to grain surface, (ii) the ionic polarization, (iii) the majority is due to the crystal defects, vacancies, and grain defects etc[28]. The increase in ε_r values with contents may be recognized by the substitution of a larger ionic radius of Sn^{4+} (~0.69 Å) cation for the lower ionic radius of Ti^{4+} (~0.64 Å) cation[29]. To increasing the bond length of complex perovskite (i.e. AB_4O_9) the larger ionic radius cation may be substituted at B-site cation. The Sn^{4+} contents greatly affected the microwave dielectric properties due to high ionic polarizibilty[30,31]. The maximum dielectric constant is obtained at x = 0.5 at maximum relative density (i.e. at low porosity). Because charge carriers need a medium to propagate and hence dielectric constant decreases with increasing material porosity[32]. Tanδ decreases with frequency due to the space charge polarization in all samples. At the lowest frequency, the maximum tangent loss occurs due to the presence of defects, impurities, and porosity in the ceramic

samples[33]. The variation of quality factor (Q_f) and relative density (%) of $Ba(Ti_{1-x}Sn_x)_4O_9$ sintered ceramics as a function of composition (x) is shown in Figure 6. Initially, the quality factor decreased from 9264.49 to 5681.16 with increasing Sn4+ content (from 0 to 0.3). The observed decrease in the value of Q_f may be recognized due to the substitution of larger Sn^{4+} cation on the B- site, contributing to harmonic vibrational modes[34] and another reason may be the phase transition. Furthermore, an increase in contents leads to giving a high Q_f value, which may occur due to (i) the phonon modes of B-site harmonic (ii) relative density is increased as Sn^{4+} content increased as shown in Figure 6 (in blue color).

The variation of ac conductivity of $Ba(Ti_{1-x}Sn_x)_4O_9$, $0 \leq x \leq 0.7$ sintered ceramics versus frequency is shown in Figure 7. It is clear from the graph that ac conductivity depends upon the frequency and does not show any significant variation at the lowest frequency. The maximum value of ac conductivity at a lower frequency may be due to the rising state of localization in the hopping process. By the application of electric field, the hopping frequency of charge carrier increased which result in the highest value of ac conductivity towards the high-frequency region[35].

Conclusion

A compound of $Ba(Ti_{1-x}Sn_x)_4O_9$, $(0 \leq x \leq 0.7)$ ceramics were fabricated through a conventional or mixed-oxide route. The average crystallite size of these ceramics lies in the range of 30-90 nm with structure change from orthorhombic (space group = Pnmm) to Tetragonal (P4*mm*). Sintered ceramics attained 99.5% of the theoretical density at content (x = 0.5) and fine grain growth. Photoluminescence confirms that the present state of localization within the bandgap may affect the structural order/disorder. The dielectric properties of sintered ceramics samples showed ε_r = 57.29, and high Q_f = 11,852. The increase in ac conductivity is due to the hopping mechanism. Based on the above-obtained results, these ceramic materials can be used for filter applications.

Declarations

Acknowledgment

Author **Khaled Althubeiti** is thankful to Researcher Supporting Project **(TURSP-2020/241)** at **Taif University** for the financial support.

Author contributions

Asad Ali and Abid Zaman prepared samples and write the manuscript. Sarir Uddin helps in measurements. Zafar Iqbal supervise this research. Madan Lal and Khaled Althubeiti did the final writing-review, corrections, and editing. All the authors read and approve the final manuscript.

Competing interests

The authors declare that they have no competing interests.

Data availability

The data of this study are available from the corresponding author upon reasonable request.

References

1 Richtmyer, R. Dielectric resonators. *Journal of Applied Physics* **10**, 391-398 (1939).

2 Sebastian, M. T. *Dielectric materials for wireless communication*. (Elsevier, 2010).

3 áVijay Kumar, H. & áMuralidhar Nayak, M. A highly efficient iron doped BaTiO 3 nanocatalyst for the catalytic reduction of nitrobenzene to azoxybenzene. *RSC Advances* **4**, 18881-18884 (2014).

4 Kumar, S. & Varma, K. Dielectric relaxation in bismuth layer-structured BaBi4Ti4O15 ferroelectric ceramics. *Current Applied Physics* **11**, 203-210 (2011).

5 Patel, S. *et al.* Tuning of dielectric, pyroelectric and ferroelectric properties of 0.715 Bi0. 5Na0. 5TiO3-0.065 BaTiO3-0.22 SrTiO3 ceramic by internal clamping. *AIP Advances* **5**, 087145 (2015).

6 Sebastian, M., Ubic, R. & Jantunen, H. Low-loss dielectric ceramic materials and their properties. *International Materials Reviews* **60**, 392-412 (2015).

7 Mirsaneh, M., Leisten, O. P., Zalinska, B. & Reaney, I. M. Circularly polarized dielectric-loaded antennas: current technology and future challenges. *Advanced Functional Materials* **18**, 2293-2300 (2008).

8 Muhammad, R., Iqbal, Y. & Reaney, I. M. New low loss A9B9O31 (A= La; B= Ti, Mg, Sc, Fe, Al, Ga) ceramics for microwave applications. *Journal of Alloys and Compounds* **646**, 368-371 (2015).

9 Praveena, K. & Varma, K. Ferroelectric and optical properties of Ba 5 Li 2 Ti 2 Nb 8 O 30 ceramics potential for memory applications. *Journal of Materials Science: Materials in Electronics* **25**, 3103-3108 (2014).

10 Rase, D. & Roy, R. Phase equilibria in the system BaO–TiO2. *Journal of the American Ceramic Society* **38**, 102-113 (1955).

11 O'Bryan Jr, H., Thomson Jr, J. & Plourde, J. A new BaO-TiO2 compound with temperature-stable high permittivity and low microwave loss. *Journal of the American Ceramic Society* **57**, 450-453 (1974).

12 Cernea, M. Microwave dielectric properties of BaT14O9-Nd2O3, BaT14O9-Sm2O3 and BaT14O9-WO3 ceramics. *Journal of optoelectronics and advanced materials* **9**, 3790-3794 (2007).

13 Mueller, V., Beige, H. & Abicht, H.-P. Non-Debye dielectric dispersion of barium titanate stannate in the relaxor and diffuse phase-transition state. *Applied physics letters* **84**, 1341-1343 (2004).

14 Lu, S., Xu, Z. & Chen, H. Tunability and relaxor properties of ferroelectric barium stannate titanate ceramics. *Applied Physics Letters* **85**, 5319-5321 (2004).

15 Shvartsman, V., Kleemann, W., Dec, J., Xu, Z. & Lu, S. Diffuse phase transition in Ba Ti 1− x Sn x O 3 ceramics: An intermediate state between ferroelectric and relaxor behavior. *Journal of Applied Physics* **99**, 124111 (2006).

16 Veenhuis, H. *et al.* Light-induced charge-transport properties of photorefractive barium-calcium-titanate crystals doped with rhodium. *Applied Physics B* **70**, 797-801 (2000).

17 Ma, H. *et al.* BaTi4O9 mesocrystal: Topochemical synthesis, fabrication of ceramics, and relaxor ferroelectric behavior. *Journal of Alloys and Compounds* **777**, 335-343 (2019).

18 Ali, A. *et al.* DIELECTRIC AND OPTICAL PROPERTIES OF TIN-DOPED BARIUM TETRA TITANATE CERAMICS. *Revista Romana de Materiale* **50**, 448-452 (2020).

19 Lal, M. *et al.* Study of structural and magnetoelectric properties of 1− x (Ba 0.96 Ca 0.04 TiO 3)−x (ZnFe 2 O 4) ceramic composites. *Journal of Materials Science: Materials in Electronics* **29**, 80-85 (2018).

20 Kumar, M. M., Srinivas, K. & Suryanarayana, S. Relaxor behavior in BaTiO~ 3. *Applied Physics Letters* **76**, 1330-1332 (2000).

21 Gupta, S. & Subramanian, V. Encapsulating Bi2Ti2O7 (BTO) with reduced graphene oxide (RGO): an effective strategy to enhance photocatalytic and photoelectrocatalytic activity of BTO. *ACS applied materials & interfaces* **6**, 18597-18608 (2014).

22 Sun, D. *et al.* Investigation on FTIR spectrum of barium titanate ceramics doped with alkali ions. *Ferroelectrics* **355**, 145-148 (2007).

23 Pavlović, N. & Srdić, V. V. Synthesis and structural characterization of Ce-doped bismuth titanate. *Materials Research Bulletin* **44**, 860-864 (2009).

24 Yadav, K. Optical and dielectric properties of Bi2Ti2O7/Bi4Ti3O12 nanocomposite. *Materials Today: Proceedings* **28**, 153-157 (2020).

25 Longo, V. *et al.* Structural conditions that leads to photoluminescence emission in Sr Ti O 3: An experimental and theoretical approach. *Journal of Applied Physics* **104**, 023515 (2008).

26 Leite, E. R. *et al.* The origin of photoluminescence in amorphous lead titanate. *Journal of Materials Science* **38**, 1175-1178 (2003).

27 El Marssi, M., Le Marrec, F., Lukyanchuk, I. & Karkut, M. Ferroelectric transition in an epitaxial barium titanate thin film: Raman spectroscopy and x-ray diffraction study. *Journal of applied physics* **94**, 3307-3312 (2003).

28 Kaur, M. *et al.* Effect on the dielectric properties due to In–N co-doping in ZnO particles. *Journal of Materials Science: Materials in Electronics* **32**, 8991-9004 (2021).

29 Shannon, R. D. Revised effective ionic radii and systematic studies of interatomic distances in halides and chalcogenides. *Acta crystallographica section A: crystal physics, diffraction, theoretical and general crystallography* **32**, 751-767 (1976).

30 Muhammad, R., Iqbal, Y. & Reaney, I. M. Structure and microwave dielectric properties of La 5− x Sr x Ti 4+ x Ga 1− x O 17 ceramics. *Journal of Materials Science* **50**, 3510-3516 (2015).

31 Iqbal, Y. & Muhammad, R. Microwave dielectric properties of Mg-doped SrLa 4 Ti 5 O 17 layered perovskite. *Journal of Materials Science: Materials in Electronics* **27**, 1314-1317 (2016).

32 Weng, M.-H., Liang, T.-J. & Huang, C.-L. Lowering of sintering temperature and microwave dielectric properties of BaTi4O9 ceramics prepared by the polymeric precursor method. *Journal of the European Ceramic Society* **22**, 1693-1698 (2002).

33 Das, S., Das, S. & Sutradhar, S. Effect of Gd3+ and Al3+ on optical and dielectric properties of ZnO nanoparticle prepared by two-step hydrothermal method. *Ceramics International* **43**, 6932-6941 (2017).

34 Zhou, D., Randall, C. A., Wang, H., Pang, L. X. & Yao, X. Microwave dielectric properties trends in a solid solution (Bi1− xLnx) 2Mo2O9 (Ln= La, Nd, 0.0≤ x≤ 0.2) system. *Journal of the American Ceramic Society* **92**, 2931-2936 (2009).

35 Khan, R. *et al.* Influence of oxygen vacancies on the structural, dielectric, and magnetic properties of (Mn, Co) co-doped ZnO nanostructures. *Journal of Materials Science: Materials in Electronics* **29**, 9785-9795 (2018).

Tables

Table 1. Lattice parameters of $Ba(Ti_{1-x}Sn_x)_4O_9$, $0 \le x \le 0.7$ ceramics obtained from XRD.

Composition (x)	Lattice parameters (Å)			Volume (Å^3)	Structure (space group)	Average crystallite size (D) nm
	a	b	c			
0.0	4.012	5.681	5.703	64.4	Orthorhombic (Pnmm)	90
0.3	4.024	4.024	4.045	65.1		50
0.5	4.036	4.036	4.057	65.7	Tetragonal (P4*mm*)	30
0.7	4.058	4.058	4.042	66.3		70

Table 2. Physical properties of $Ba(Ti_{1-x}Sn_x)_4O_9$, $0 \leq x \leq 0.7$ sintered ceramics.

Composition (x)	ρ_{th} (gm/cm^3)	ρ_{ex} (gm/cm^3)	ρ_{re} (%)	ϵ_r	Porosity (%)	Average grain size (µm)
0.0	5.9	4.5	76.3	30.08	23.72	10.7
0.3	4.953	4.48	90.5	37.57	9.55	6.45
0.5	5.611	5.58	99.4	57.29	0.55	2.54
0.7	5.347	5.25	98.2	46.63	1.81	5.56

Figures

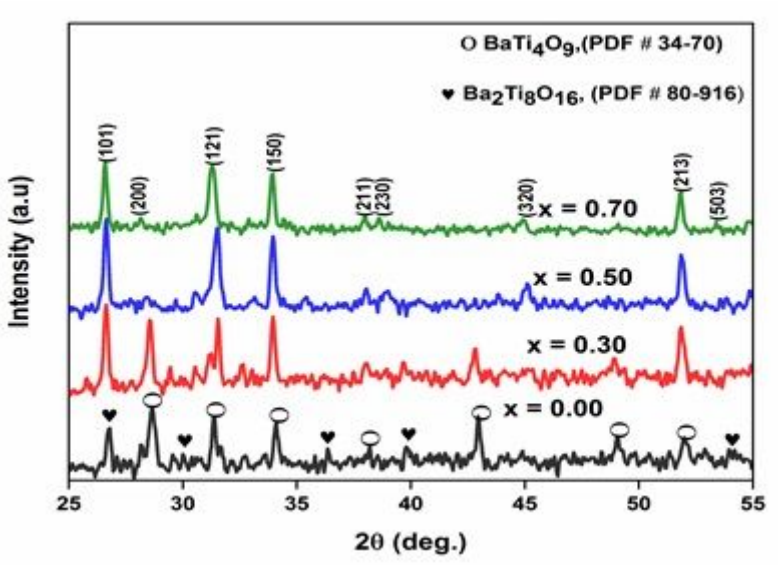

Figure 1

XRD pattern of Ba(Ti1-xSnx)4O9, $0 \leq x \leq 0.7$ ceramics.

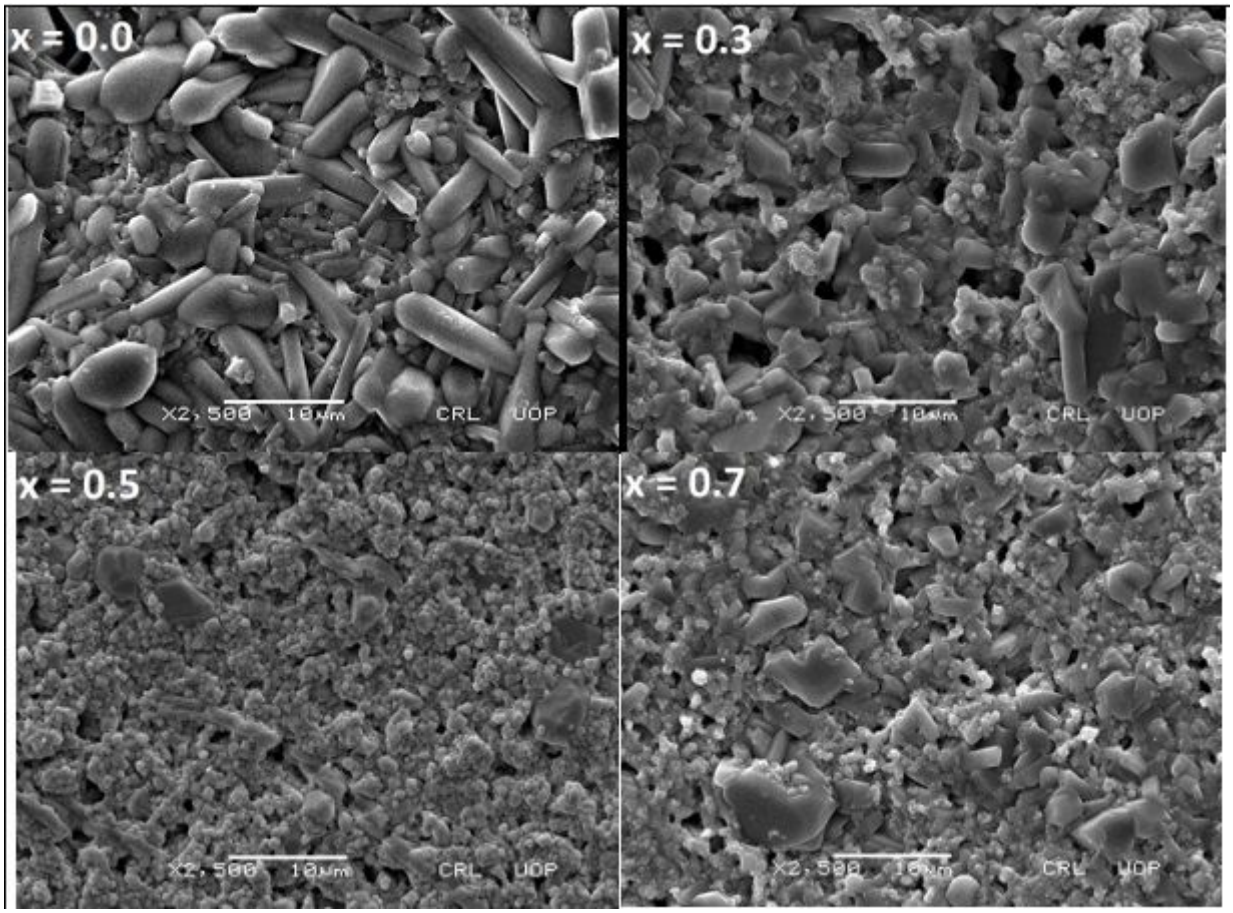

Figure 2

SEM Micrograph of Ba(Ti1-xSnx)4O9, 0 ≤ x ≤ 0.7 ceramics.

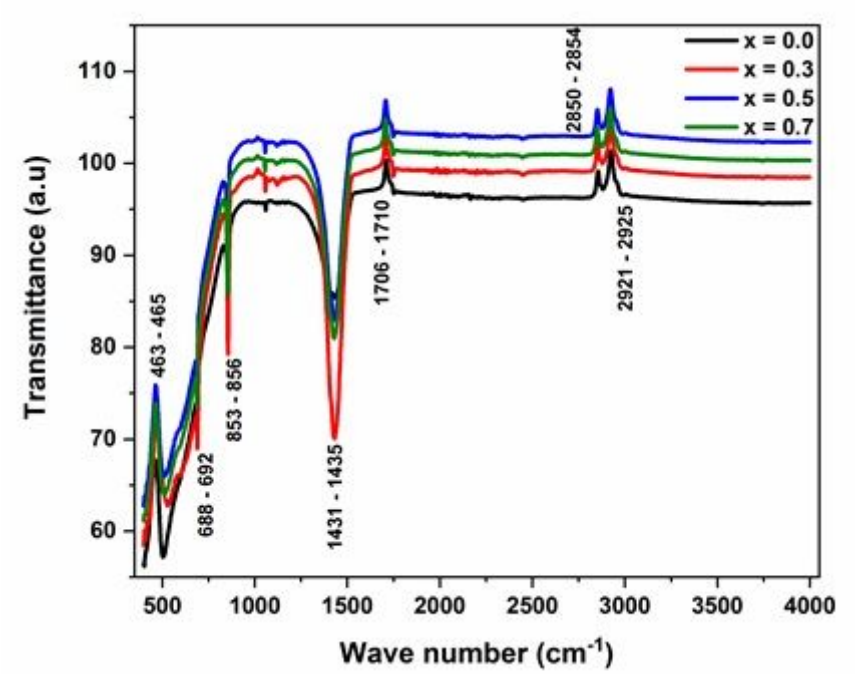

Figure 3

FTIR spectra of Ba(Ti1-xSnx)4O9, 0 ≤ x ≤ 0.7 ceramics.

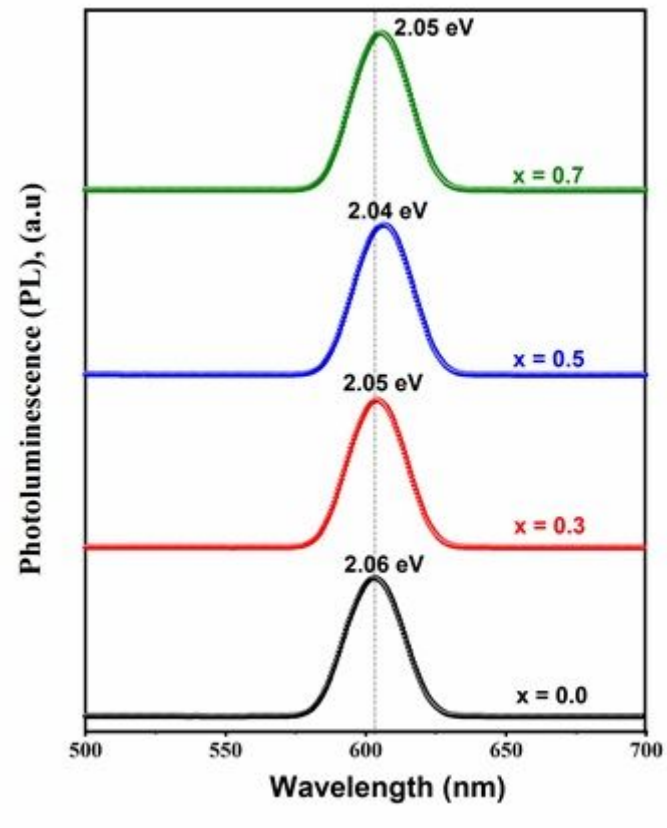

Figure 4

PL spectra of Ba(Ti1-xSnx)4O9, 0 ≤ x ≤ 0.7 ceramics.

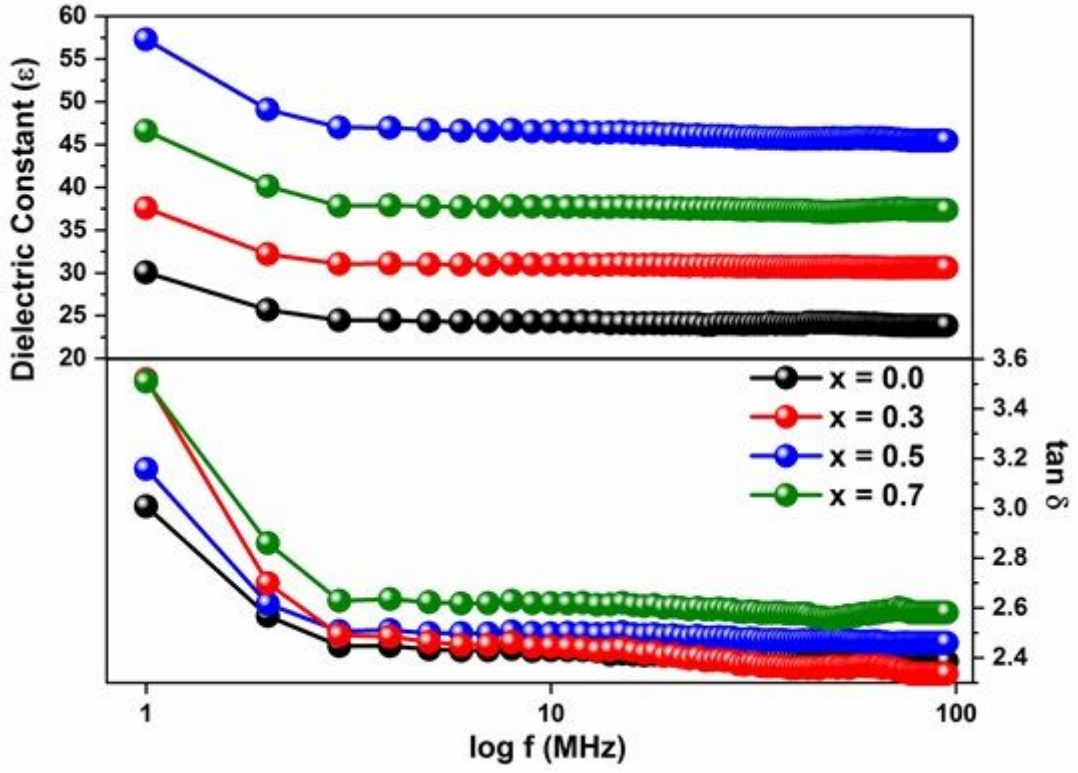

Figure 5

Frequency dependence of Dielectric constant (ε) and dielectric loss (tanδ) of Ba(Ti1-xSnx)4O9, 0 ≤ x ≤ 0.7 ceramics

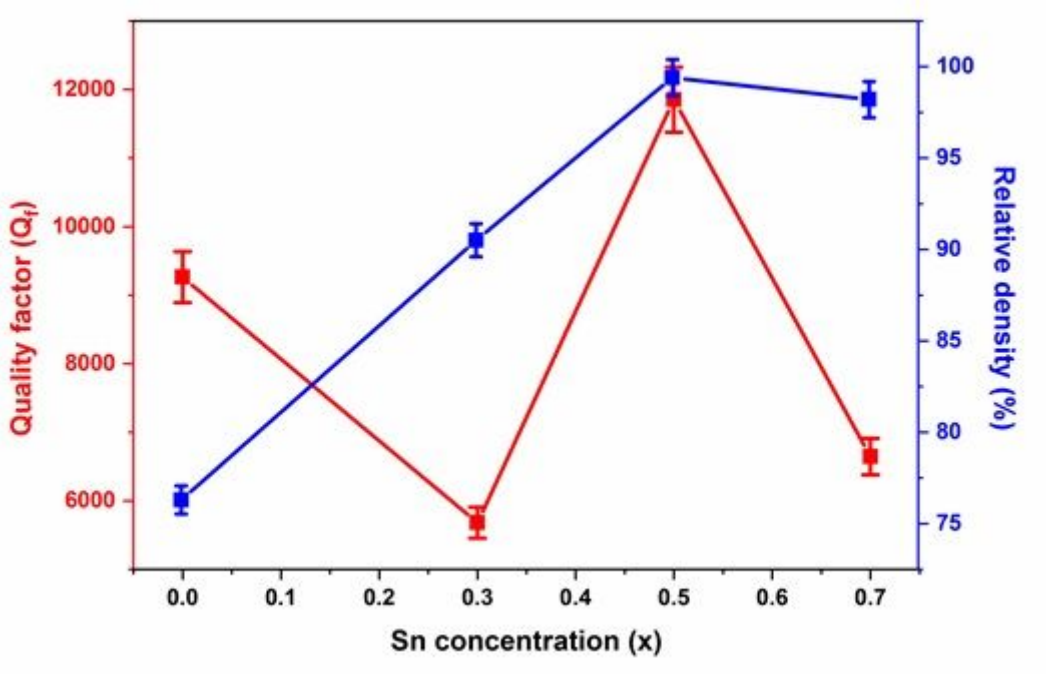

Figure 6

Variation of relative density and Quality factor (Qf) vs Sn4+ contents of Ba(Ti1-xSnx)4O9, 0 ≤ x ≤ 0.7 ceramics.

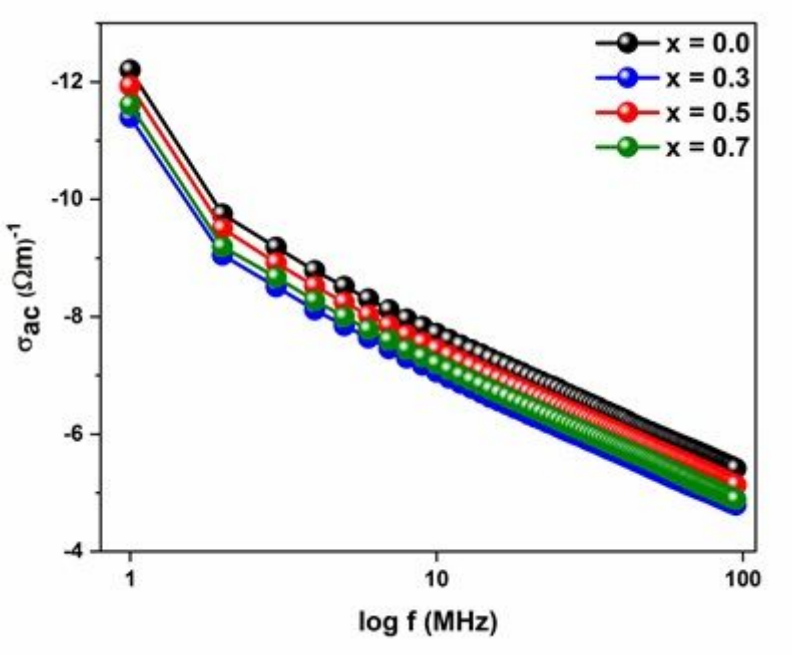

Figure 7

Variation of ac conductivity as a function of the frequency of Ba(Ti1-xSnx)4O9, 0 ≤ x ≤ 0.7 ceramics